7. International Immersive Projection Technologies Workshop
9. Eurographics Workshop on Virtual Environments (2003)
J. Deisinger, A. Kunz (Editors)

A Comprehensive Calibration and Registration Procedure for the Visual Haptic Workbench

Milan Ikits, Charles D. Hansen and Christopher R. Johnson

Scientific Computing and Imaging Institute, University of Utah, Salt Lake City, Utah, U.S.A.
{ikits,hansen,crj}@sci.utah.edu

Abstract

We present a simple yet efficient calibration and registration procedure for improving the overall static display accuracy of the Visual Haptic Workbench. The procedure is used for precisely colocating the visual and haptic workspaces of the system and is divided into three stages. First, we calibrate and register the PHANToM to the display surface of the workbench. Second, we calibrate the tracking system by attaching a rigid extension between the tracker sensor and the PHANToM stylus. Third, we interactively find the remaining unknown display parameters including eye and hotspot offsets as well as a local reference frame. Initial evaluation of the approach indicates that it is possible to improve static display accuracy by at least an order of magnitude for this system.

Categories and Subject Descriptors (according to ACM CCS): H.5.2 [User Interfaces]: Input devices and strategies I.3.7 [Computer Graphics]: Virtual Reality

1. Introduction

Several applications of combined immersive visual and haptic displays can greatly benefit from accurate calibration and registration of system components. Examples include surgical simulation, planning and training, virtual prototyping, as well as scientific visualization. Unfortunately, precise registration is difficult to achieve because of the large number of factors that effect overall system accuracy. According to the model developed by Holloway for an augmented reality surgical planning system, registration error sources can be divided into four categories: data acquisition, tracking, display, and viewing errors.[13] We categorize the error sources according to whether they produce *geometric* or *optical* distortions. Geometric errors are the result of inaccurate tracking, system delay, misalignments of coordinate systems, as well as imprecise viewing and interaction parameters. Optical errors are due to the limitations of the image generation subsystem, manifested by convergence problems, display nonlinearities, aliasing, and color aberration. The fidelity of haptic rendering largely depends on the structural and dynamic characteristics of the haptic interface, the accuracy of its kinematic description, as well as the model and control algorithm used to produce the reaction forces and torques.

In this paper we focus on improving the overall static display accuracy of the Visual Haptic Workbench by reducing geometric distortions in the system. Our goal is to develop a comprehensive procedure that allows the simultaneous calibration and coregistration of the system components. The procedure needs to be accurate, fast, robust, and flexible enough to be applied to other similar configurations. From these requirements it follows that the calibration techniques should not rely on external metrology and be composed of a series of simple operations.

2. Previous Work

The majority of previous work has concentrated on registration issues for HMD and desktop augmented reality systems. Pioneering research was conducted at the University of North Carolina throughout the past decade, primarily focusing on head-mounted displays.[19, 8, 2, 20, 13] Deering presented a careful examination of factors influencing the accuracy of a desktop head-tracked stereo CRT display.[6] Hodges and Davis discussed stereoscopic viewing in detail along with several hardware and software limitations and artifacts.[10]

A registration procedure utilizing a precision surveying theodolite was developed for colocating the visual and hap-

tic workspaces of the nanoWorkbench.[9] The authors mentioned that a better approach would be to develop a semi-automatic calibration method by attaching a rigid extension to the PHANToM stylus. This is the approach we pursue in this paper. Summers *et al.* developed a calibration methodology for augmented reality experimental testbeds and demonstrated its validity for the Virtual Hand Laboratory.[21] The Reachin API has a built-in calibration procedure that can be used to align a virtual tool representation with the PHANToM stylus.[1] Note that only a few attempts have been made to characterize and improve the positioning accuracy of the PHANToM.[18, 24, 4]

Tuceryan *et al.* introduced a method for pointer and object calibration for a monitor-based augmented reality system.[22] More recently, Fuhrmann *et al.* developed a comprehensive registration procedure suitable for both head-mounted and head-tracked displays.[7] In this work we adapt their techniques of hotspot, world, and viewpoint calibration to our configuration.

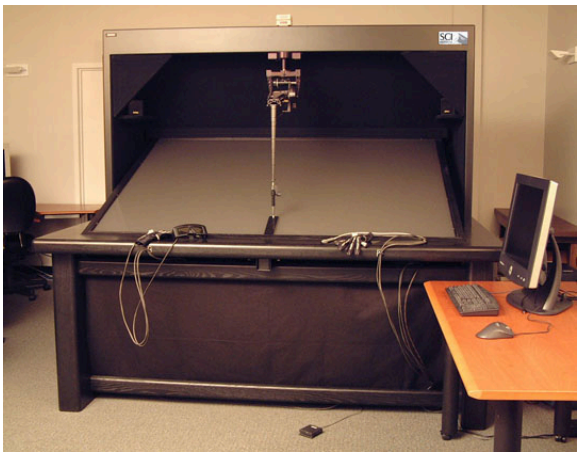

Figure 1: *The Visual Haptic Workbench comprises a large workspace PHANToM mounted on top of an Immersive Workbench.*

3. The Visual Haptic Workbench

The Visual Haptic Workbench is a testbed system developed primarily for haptic immersive scientific visualization.[3] It is composed of a SensAble PHANToM 3.0L mounted on top of a Fakespace Immersive Workbench, shown in Figure 1. Head, hand, and stylus pose measurements are provided by a Polhemus Fastrak magnetic position tracker. Stereo images are generated by an Electrohome Marquee 9500LC projector and are reflected via folded optics onto the back of the nonlinear diffusion surface of the workbench. A pair of Stereographics CrystalEyes LCD shutter glasses is used for fusing the stereo images, strobed at a 120Hz refresh rate. In a typical scenario, the user's dominant hand manipulates the PHANToM stylus to experience haptic feedback and the subdominant hand is used for system control tasks such as navigating a menu interface. A pair of Fakespace Pinch Gloves and a pair of 5DT Data Gloves are provided for implementing more complex interaction techniques. We have constructed a registration apparatus that allows the user to place the PHANToM in a fixed pose on the surface of the workbench during encoder initialization. The system is currently driven by a dual Pentium 4 Dell PC with 2GB of memory and an ATI Radeon 9700 graphics board.

4. Components of the Registration Procedure

Let us consider the possible sources of geometric errors for our setup, as illustrated in Figure 2. The errors include the individual device workspace distortions and the unknown rigid body transformations between the respective coordinate frames: the tracker transmitter $\mathbf{R}_0$, the screen location $\mathbf{S}$, the PHANToM base $\mathbf{P}_0$, the head and eye locations $\mathbf{H}$, $\mathbf{e}_L$ and $\mathbf{e}_R$, as well as the stylus tip $\mathbf{T}$ and the pinch spot $\mathbf{C}$ relative to the receiver frames $\mathbf{R}_1$ and $\mathbf{R}_3$. Device inaccuracies are captured by measurement errors $\Delta\mathbf{f}_T$ and $\Delta\mathbf{f}_P$, where $\mathbf{f}_{T_i} = \mathbf{T}_{R_0 \to R_i}$ and $\mathbf{f}_P = \mathbf{T}_{P_0 \to P_6}$ represent the position and orientation readings for tracker receiver i and the PHANToM, respectively. These transformations and parameters are summarized in Table 1 along with the corresponding calibration processes as well as the nominal accuracies, similarly to Tuceryan *et al.*[22] Nominal accuracy is defined by what we can achieve without calibration and via simple ad-hoc registration techniques. Our goal is to reduce the overall registration error to a few millimeters. Note that the local reference frame $\mathbf{L}$ is application dependent and has to be defined after the transformations between the tracker and PHANToM bases as well as the screen coordinate system have been found.

Calibration techniques aim to reduce discrepancies by characterizing the error of the underlying model of pose measurement. For magnetic tracking devices this involves finding a suitable parametric description of the magnetic field distortion and a way of extracting the model parameters from a number of calibration measurements.[15] Alternatively, a lookup table (LUT) can be constructed that captures the discrepancies.[16] For haptic devices a suitable model already exists, but it is typically augmented with additional parameters such as joint gains and offsets.[11]

Registration is concerned with finding the remaining unknown display parameters including the relative transformations between the individual workspaces. Some of these parameters can be measured accurately, *e.g.* the screen width w and height h. Others might need to be controlled explicitly, such as the eye separation distance e to bring objects into the fusible stereoscopic range.[26] Other values are generally not very accurately measured, such as the head reference frame $\mathbf{H}$, the projection centers in the user's eyes $\mathbf{e}_L$ and $\mathbf{e}_R$, and the interaction device hotspots, *e.g.* the stylus tip $\mathbf{T}$ rel-

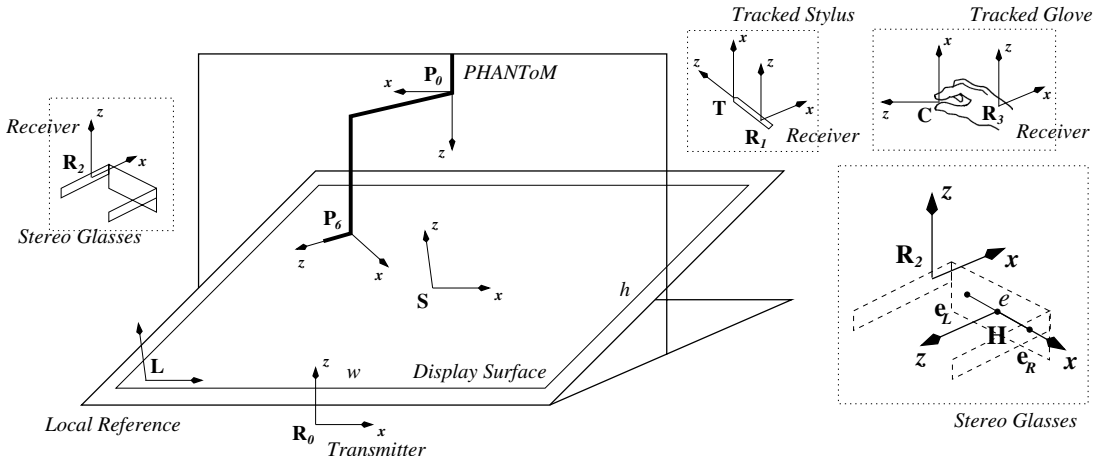

Figure 2: *Coordinate frames effecting display accuracy of the Visual Haptic Workbench. Possible sources of error include individual device workspace distortions and misalignments of the respective coordinate systems.*

Transformation	Description	Nature	Calibration Process	Nominal Accuracy
w, h	Screen width and height	fixed	Projector	1-2 mm
$\mathbf{P}_0 \rightarrow \mathbf{P}_6$	PHANToM pose	varying	PHANToM	10-60 mm
$\mathbf{S} \rightarrow \mathbf{P}_0$	Screen-to-PHANToM	fixed	PHANToM	10-50 mm
$\mathbf{R}_0 \rightarrow \mathbf{R}_i$	Tracker pose	varying	Tracker	5-100 mm
$\mathbf{R}_0 \rightarrow \mathbf{P}_0$	Tracker-to-PHANToM	fixed	Tracker	10-50 mm
$\mathbf{R}_1 \rightarrow \mathbf{T}$	Receiver-to-Tip	fixed	Hotspot	2-5 mm
$\mathbf{R}_3 \rightarrow \mathbf{C}$	Receiver-to-Pinch	user-specific	Hotspot	2-5 mm
$\mathbf{R}_2 \rightarrow \mathbf{H}$	Receiver-to-Head	user-specific	View	2-5 mm
e	Eye separation	user-specific	View	1-2 mm
$\mathbf{S} \rightarrow \mathbf{L}$	Screen-to-Local	application-specific	World	2-5 mm

Table 1: *Summary of relevant coordinate transformations and parameters.*

ative to the receiver frame $\mathbf{R}_1$. For improved interaction it is desirable to obtain user-specific measurements of these parameters. Since hotspot, view, and world calibration assumes that accurate tracking and display are available, we need to calibrate the projector, the PHANToM, and the tracker before finding the remaining unknown display parameters of the system.

4.1. Projector Calibration

The analog projector used in our setup has reasonable electronic adjustment and tuning capabilities. It is important to make sure that the size of the display window is measured with the desired accuracy. Precise linearization of the display can be achieved by overlaying a transparent sheet with grid lines on the screen surface.[5]

4.2. PHANToM Calibration

There are two reasons for the poor positioning accuracy of the PHANToM. First, the standard procedure for initializing the optical encoders is based on manually holding the arm in a reset position, as shown in Figure 3. This can hardly be accomplished and repeated in a precise manner. Although a reset arm is available for the PHANToM 3.0L, it cannot be used in the overhead configuration. Thus, a custom calibration apparatus is needed that allows the user to quickly place the end-effector to a fixed known location within the workspace of the device. Second, the pose and force calculations within the GHOST and BasicIO libraries are based on the nominal kinematic model of the device, which is different from the actual realization. For example, the stylus end-effector in our setup has visually apparent misalignment, because rotation axes $\mathbf{z}_4$ and $\mathbf{z}_5$ do not meet at a right angle. These error sources typically result in a total discrepancy of about $10-60$ mm and a few degrees at the stylus endpoint.

To find more accurate kinematic parameters, we calibrate the device by taking a number of joint angle measurements while constraining the endpoint to a grid placed on top of the display surface of the workbench. We augment the end-effector with a special probe and define a base reference

frame $\mathbf{P}_{-1}$ on the grid. Following the notation of Hollerbach and Wampler, the resulting mixed Denavit-Hartenberg-Hayati parameters are collected in Table 2.[11] Values not estimated by the calibration procedure are indicated by a boldface font.

The calibrated parameters are found via nonlinear least-squares estimation by iteratively minimizing the discrepancy between the Cartesian coordinates of the grid points and the calibration tool endpoint:

$$\Delta\mathbf{p}^i = \mathbf{p}_0^i - \mathbf{p}^i(\phi^k, \psi^i) = \frac{\partial \mathbf{p}^i}{\partial \phi}(\phi^k, \psi^i)\,\Delta\phi = \mathbf{J}^i\,\Delta\phi \quad (1)$$

The estimation algorithm finds parameter corrections $\Delta\phi$ at iteration step k, where $\mathbf{p}^i(\phi^k)$ represents measurement location i expressed in the surface frame, computed from the forward kinematics of the device using the current parameter estimate ϕ^k and raw joint sensor readings ψ^i. Further details of robot calibration including measurement pose selection and statistical analysis of the results are given by Hollerbach and Wampler.[11] To find the transformation between the reference coordinate system $\mathbf{P}_{-1}$ and the screen frame $\mathbf{S}$, we measure the distances between the corners of the display area and the calibration grid.

j	d_j	a_j	α_j	β_j	γ_j
0	d_0	a_0	α_0	**0**	γ_0
1	d_1	0.0	−90.0	**0**	γ_1
2	**0**	457.2	0.0	0.0	0.0
3	0.0	0.0	−90.0	**0**	0.0
4	−457.2	0.0	90.0	**0**	0.0
5	0.0	0.0	−90.0	**0**	90.0
6	**0**	**0**	**180**	**0**	**90**
7	d_7	a_7	**0**	**0**	γ_7

Table 2: *Nominal parameters of the PHANToM for grid calibration. Distances and angles are given in millimeters and degrees. Fixed parameters are indicated in boldface.*

4.3. Tracker Calibration

Magnetic tracker distortion is a major contributing factor to visual registration errors. Without calibration, head-tracking errors can be as large as 70 mm in our configuration. This can be reduced effectively to about 5 mm.[15] Note, however, that there is no need to sample the whole visual workspace uniformly to correct for the distortion everywhere. Since users do not typically move away much from the central position in front of the workbench, it is reasonable to concentrate only on the frequently used regions of the workspace. These include the central viewing area located at head-level above the tracker transmitter and the interaction region above the display surface.

We adapt the method of Livingston and State[16] for determining the magnetic field distortion within these areas. By attaching a rigid extension between the PHANToM stylus and the tracker receiver, a large number of measurements can be collected within a short amount of time. The length of the link and the transformation between the tracker and PHANToM bases can be found from measurements taken close to the magnetic source, where the distortion is negligible.[14, 15] The collected measurements are used to construct an explicit correction table from which the distortion is computed via linear tetrahedral interpolation.

4.4. Hotspot, View and World Calibration

The remaining parameters can be found via an interactive procedure. Some of these parameters do not depend on the user and are measured only once. Others may need to be adjusted at the beginning and during application runs.

There are two ways to define interaction hotspots. One is to touch the device to a precisely measured point.[22] The other is to constrain it to an unknown location and rotate it around on a hemisphere while taking measurements with the tracker.[7] The former works better for the pinch spot $\mathbf{C}$, the latter can be used to find the stylus tip $\mathbf{T}$. The hotspot coordinate axes are usually aligned with the receiver frame or can be found from a procedure similar to world calibration. Note that for the PHANToM, the intersection of the last three joint axes define the location where forces are applied. This point is obtained from the PHANToM calibration procedure.

In our setup the visual representation of hotspots need to be offset from the physical locations, otherwise occlusion cues break the stereo illusion. Paljic *et al.* reported that this is usually not a problem and users can tolerate a small offset between the physical and virtual interaction points for typical navigation and manipulation tasks.[17]

It is not completely clear which point in the eye should be considered the modeled center of projection. Rolland *et al.* suggested that using the entrance pupil is more realistic than the first nodal point proposed by Deering.[20, 6] Holloway as well as Vaissie *et al.* showed that choosing the center of rotation minimizes depth errors.[13, 23] Computing the viewpoint offset from aligning two or more precisely known physical or virtual targets has been reported to provide sufficient visual registration accuracy.[2, 7] Thus, we find the receiver-to-eye offsets $\mathbf{e}_L$ and $\mathbf{e}_R$ by visually superimposing the PHANToM calibration tool on physical markers on the screen. From these two offsets the head reference frame $\mathbf{H}$ and the eye separation distance e can be calculated. Note that we can also measure e with a ruler or more precisely with a pupillometer, which can be used to verify the accuracy of this technique.

Finally, the local world reference frame is defined by asking the user to specify its origin, handedness, and directions

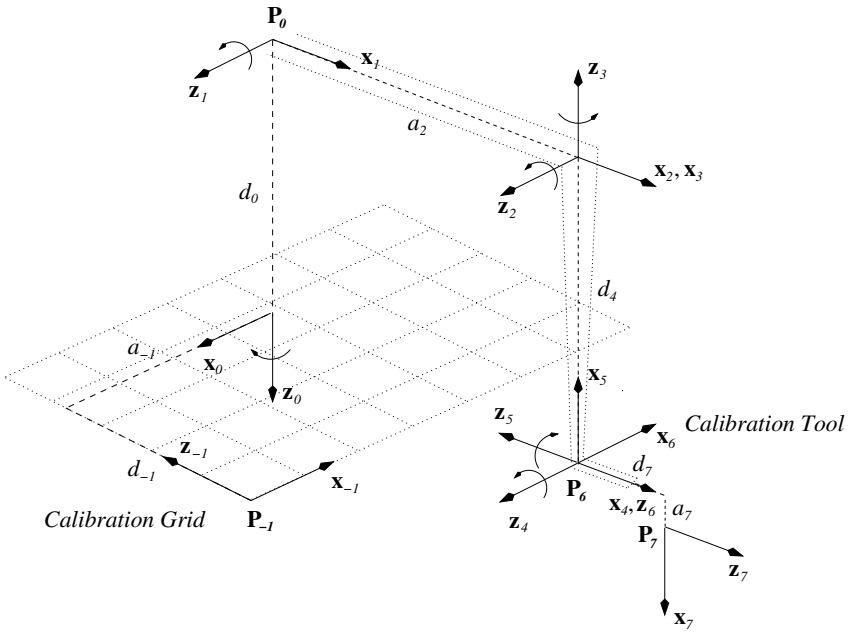

Figure 3: *Kinematic model of the PHANToM 3.0L mounted in the overhead configuration (T model). The stylus is augmented with a calibration tool for taking measurements on the display surface of the workbench.*

of two coordinate axes.[7] Typically, the axes are aligned with the axes of either the screen or the tracker coordinate system.

A related question that has not been completely investigated in head-tracked stereoscopic environments is the effect of viewing and tracking errors on the perceived virtual world. It is well known that head orientation errors do not result in as severe consequences for HTDs as they do for HMDs. It has been reported that head rotation errors cause the displayed objects to appear to distort and move slightly, and that tracking full head pose is still necessary to avoid having to keep the head in the correct orientation.[9] In the following section, we derive simple analytic formulas that yield more insight into the nature of the visual distortion.

5. Analysis of Visual Distortion Effects due to Tracking and Viewing Errors

The following analysis based on the work of Holloway and Wartell *et al.* demonstrates how tracking and viewing errors influence the perceived virtual world.[12, 25, 26] To simplify the derivations we consider the two-dimensional parallel case here.

Figure 4 illustrates the effect of head-tracking and viewing errors in general. The vector between the actual eye positions **A** and **D** is parallel with the projection line. The modeled eye locations **B** and **C** are displaced due to head-tracking and viewing errors. Thus, the desired virtual location **E** is displaced to **F** resulting in a distortion of the visual workspace. We are interested in characterizing the error between these points as a function of tracker and viewing distortion. The perceived location **F** is related to the parameters of the model by:[12, 25]

$$F_x = \frac{A_z D_x G_x - A_x D_z H_x + (D_z - A_z) G_x H_x}{A_z D_x - A_x D_z + D_z G_x - A_z H_x} \quad (2)$$

$$F_z = \frac{A_z D_z G_x - A_z D_z H_x}{A_z D_x - A_x D_z + D_z G_x - A_z H_x} \quad (3)$$

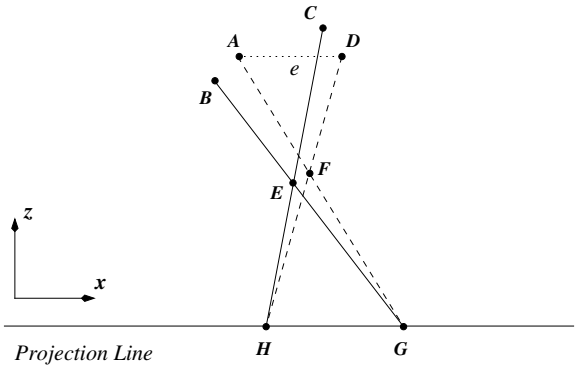

Figure 4: *Parameters of the analytic model. The actual eye separation vector is parallel with the projection line.*

where:

$$H_x = \frac{(E_x - C_x)C_z}{C_z - E_z} + C_x \quad (4)$$

$$G_x = \frac{(E_x - B_x)B_z}{B_z - E_z} + B_x \quad (5)$$

We consider the effect of position and orientation errors separately. For position errors the modeled and actual eye locations are related by:

$$\mathbf{B} = \mathbf{A} + \varepsilon \quad (6)$$

$$\mathbf{C} = \mathbf{D} + \varepsilon \quad (7)$$

where ε is the position error of the head tracker. Knowing that $A_z = D_z$, it is easy show that the error between the modeled and perceived locations is:

$$\|\mathbf{F} - \mathbf{E}\| = \frac{|E_z|}{|A_z + \varepsilon_z|}\|\varepsilon\| \quad (8)$$

Suppose that the tracking error is significantly smaller than the eye distance from the projection line and that the point on the object is between the eye separation vector and its reflection over the projection line:

$$|E_z| \leq \lambda\,|A_z| \quad (9)$$

$$|A_z| - |\varepsilon_z| \leq \kappa\,|A_z| \quad (10)$$

Now we can *bound* the perceived visual distortion by the tracking error:

$$\|\mathbf{F} - \mathbf{E}\| \leq \frac{\lambda}{\kappa}\|\varepsilon\| \quad (11)$$

Typical values for the constants are $\lambda \leq 0.6$ and $\kappa \geq 0.9$. Thus, if the displayed objects are within the fusible stereoscopic range, they are distorted by no less than the head position error. Another consequence of equation (8) is that the distortion is a function of the object distance from the projection line, therefore the visual error is smaller near the display surface. Holloway arrived at the same conclusion in his analysis. The effect is also clearly shown in Figure 5.

Head orientation errors result in a more complex distortion of the perceived space. It can be shown that if we consider the component of the orientation error along the z axis only:

$$B_x = A_x \quad (12)$$

$$B_z = A_z - \varepsilon \quad (13)$$

$$C_x = D_x \quad (14)$$

$$C_z = D_z + \varepsilon \quad (15)$$

and assuming that the rotation error is small compared to the distance between the eye midpoint $\mathbf{I} = (\mathbf{A} + \mathbf{D})/2$ and the object point $\mathbf{E}$, we can approximate the distortion by:

$$\|\mathbf{F} - \mathbf{E}\| \approx \frac{|E_z|}{|A_z|}\frac{I_x - E_x}{e/2}\,|\varepsilon| \quad (16)$$

The region where the effect of head orientation errors can be bounded is characterized by:

$$\frac{|E_z|}{|A_z|}\frac{I_x - E_x}{e/2} \leq \mu \quad (17)$$

for a given error limit μ. This is a diamond shape region centered around the intersection of the bisector line between the eyes and the projection line, as shown in Figure 6.

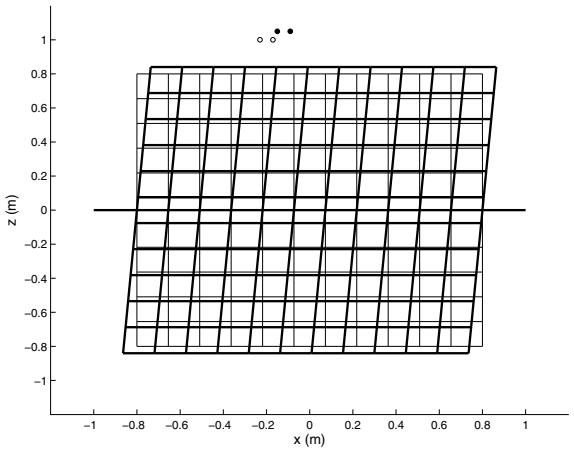

Figure 5: *The effect of head position error. The perceived virtual space appears expanded and sheared. The modeled and true eye locations are represented by the empty and filled circles, respectively. The thin grid indicates the true workspace, the thick one is the perceived counterpart.*

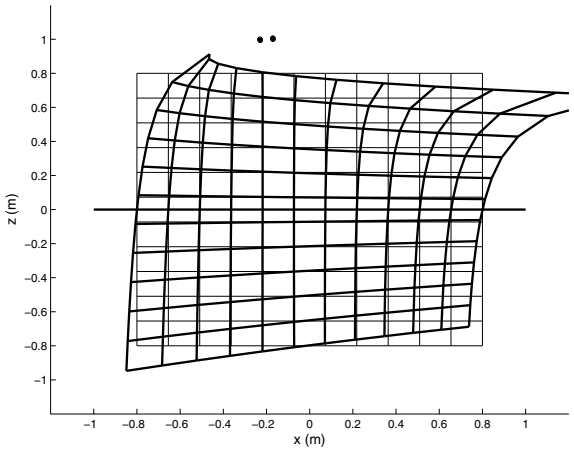

Figure 6: *The effect of head orientation errors (+10 deg). Notice the diamond shape region where the distortion is not as severe.*

Notice that the perceived distortion grows rapidly outside this area. Fortunately, users typically focus straight ahead

to the more accurate region. It can be shown that a similar diamond shape area is obtained for the non-parallel case. The severely distorted region close to the eyes is not visible, but the distortion behind the display may be noticeable. For our applications, however, we are mostly concerned with the workspace in front of the projection surface.

6. Evaluation of PHANToM Calibration

The most important component of the procedure is the calibration of the PHANToM, since the remaining steps assume that accurate tracking is available. To verify the feasibility of our approach we collected measurements at $5''$ intervals on an 8×5 grid placed on top of the workbench surface. During data collection we randomly selected the orientation of the measuring probe and made sure it covered the range of possible joint motion of the wrist. Only 37 of the 40 points were reachable by the device. Data acquisition could conveniently be performed at a three points per minute rate. The estimated accuracy of our measurement apparatus is 0.5 ± 0.5 mm.

We found that the location of the grid has a significant influence on the accuracy of the parameter estimation. The condition number of the aggregate parameter Jacobian matrix $\mathbf{J}$ is a good indicator of observability.[11] The rule of thumb is that if the condition number is well over 100, the least-squares fit will not yield a reliable set of parameter estimates. Unfortunately, we found that the location of the workbench screen is not appropriate for precise calibration, because the poor observability of the combination of certain parameters result in a condition number larger than 150. Thus, we had to place another grid nearly perpendicular to the bench surface on which 20 more samples were collected. Note that the parameters given in Table 2 need to be augmented to account for the extra reference frame of the second grid. Using the combination of the two sets of measurements the condition number was reduced to 70.

Figure 7 shows the deviations from the grid points using the nominal model, applying joint angle offset correction as well as full calibration. Precise joint angle offsets significantly improve the positioning accuracy of the device by reducing the error from $30-60$ mm to about 10 mm. Using the more accurate kinematic model further improves positioning accuracy to about 1 mm, turning the PHANToM into a sufficiently accurate position tracking device for the remaining calibration and registration steps. We noticed a similar improvement when omitting every third sample from the calibration and using them for validating the approach.

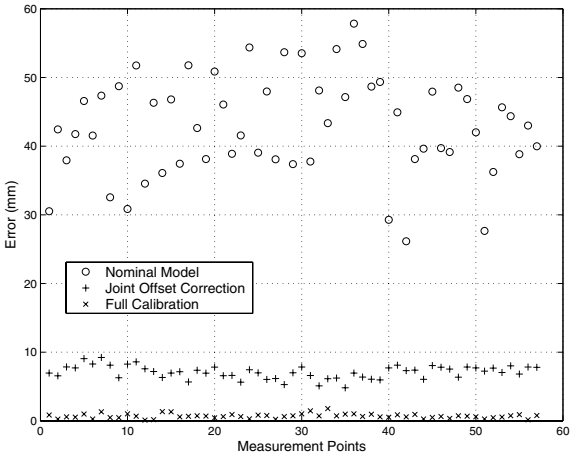

Figure 7: *Errors between the tool endpoint and the calibration grid points. The figure shows the effect of correcting joint angle offsets and how inaccurate the nominal model is.*

7. Conclusions and Future Work

We have described a comprehensive calibration and registration procedure for the Visual Haptic Workbench. A major advantage of the approach is that it does not rely on external metrology. Typically, robot calibration techniques require an accurate optical position tracking device, which we do not have in our configuration. We have chosen the order of the calibration processes such that only the components of the system and a simple measurement apparatus are needed for the simultaneous calibration and coregistration of the various workspaces. An further advantage of the procedure is that it supports rapid and convenient data acquisition.

We believe it is fairly easy to extend the approach to other configurations. Note that it is not necessary for the haptic device to reach the display, since any other planar surface can be used for calibration. It would be particularly interesting to evaluate the accuracy of a desktop system, such as the widely-used Reachin Display.

Evaluation of the remaining components of the procedure is in progress. Even though we are limited by the display and tracking components of our system, we anticipate that it is possible to reduce registration errors to within a few millimeters, which is significantly better than previously reported results.[9] The analysis of the visual effects of tracking and viewing errors presented here forms the basis for quantifying the degree of colocation between the visual and haptic workspaces. Note, however, that a more complete analysis need to take into account of the characteristics of the human visual and kinesthetic sensory systems.

Unfortunately, correcting for static errors only partially solves the registration problem. It is well known, especially to users of AR setups, that system delay is the largest contributing source of registration errors.[13] Dynamic registration accuracy can be improved by predictive filtering, synchronized display methods, and careful runtime mapping of the application components to the underlying hardware configuration.

Acknowledgements

The authors thank J. Dean Brederson for designing the system and initial conversations leading to this research. Support was kindly provided by NSF Grant ACI-9978063 and the DOE Advanced Visualization Technology Center.

References

1. Reachin Technologies AB. `http://www.reachin.se/`.
2. R. Azuma and G. Bishop. Improving Static and Dynamic Registration in an Optical See-Through HMD. In *Proceedings ACM SIGGRAPH*, pages 197–204, Orlando, Florida, July 1994.
3. J. D. Brederson, M. Ikits, C. R. Johnson, and C. D. Hansen. The Visual Haptic Workbench. In *Proceedings PHANToM Users Group Workshop*, Aspen, Colorado, Oct. 2000.
4. M. C. Çavuşoğlu, D. Feygin, and F. Tendick. Critical Study of the Mechanical and Electrical Properties of the PHANToM Haptic Interface and Improvements for High Performance Control. *Presence: Teleoperators and Virtual Environments*, 11(6):555–568, 2002.
5. M. Czernuszenko, D. J. Sandin, and T. A. DeFanti. Line of Sight Method for Tracker Calibration in Projection-Based VR Systems. In *Proceedings Immersive Projection Technology Workshop*, Ames, Iowa, May 1998.
6. M. Deering. High Resolution Virtual Reality. In *Proceedings ACM SIGGRAPH*, pages 195–202, Chicago, Illinois, July 1992.
7. A. L. Fuhrmann, R. Splechtna, and J. Přikryl. Comprehensive Calibration and Registration Procedures for Augmented Reality. In *Proceedings Eurographics Workshop on Virtual Environments*, pages 219–228, Stuttgart, Germany, May 2001.
8. S. Gottschalk and J. F. Hughes. Autocalibration for Virtual Environments Tracking Hardware. In *Proceedings ACM SIGGRAPH*, pages 65–72, Anaheim, California, Aug. 1993.
9. B. Grant, A. Helser, and R. M. Taylor II. Adding Force Display to a Stereoscopic Head-Tracked Projection Display. In *Proceedings IEEE Virtual Reality Annual International Symposium*, pages 81–88, Atlanta, Georgia, Mar. 1998.
10. L. F. Hodges and E. T. Davis. Geometric Considerations for Stereoscopic Virtual Environments. *Presence: Teleoperators and Virtual Environments*, 2(1):34–43, 1993.
11. J. M. Hollerbach and C. W. Wampler. The Calibration Index and Taxonomy of Robot Kinematic Calibration Methods. *International Journal of Robotics Research*, 15(6):573–591, 1996.
12. R. L. Holloway. *Registration Errors in Augmented Reality Systems*. PhD thesis, Department of Computer Science, University of North Carolina at Chapel Hill, 1995.
13. R. L. Holloway. Registration Error Analysis for Augmented Reality. *Presence: Teleoperators and Virtual Environments*, 6(4):413–432, 1997.
14. M. Ikits. Coregistration of Pose Measurement Devices Using Nonlinear Least Squares Parameter Estimation. Technical Report UUCS-00-018, School of Computing, University of Utah, Dec. 2000.
15. M. Ikits, J. D. Brederson, C. D. Hansen, and J. M. Hollerbach. An Improved Calibration Framework for Electromagnetic Tracking Devices. In *Proceedings IEEE Virtual Reality*, pages 63–70, Yokohama, Japan, Mar. 2001.
16. M. A. Livingston and A. State. Magnetic Tracker Calibration for Improved Augmented Reality Registration. *Presence: Teleoperators and Virtual Environments*, 6(5):532–546, 1997.
17. A. Paljic, J.-M. Burkhardt, and S. Coquillart. A Study of Distance of Manipulation on the Responsive Workbench. In *Proceedings Immersive Projection Technology Workshop*, Orlando, Florida, Mar. 2002.
18. K. Reinig, R. Tracy, H. Gilmore, and T. Mahalik. Some Calibration Information for a PHANToM 1.5 A. In *Proceedings PHANToM Users Group Workshop*, Dedham, Massachusetts, Oct. 1997.
19. W. Robinett and J. P. Rolland. A Computational Model for the Stereoscopic Optics of a Head-Mounted Display. *Presence: Teleoperators and Virtual Environments*, 1(1):45–62, 1991.
20. J. P. Rolland, D. Ariely, and W. Gibson. Towards Quantifying Depth and Size Perception in Virtual Environments. *Presence: Teleoperators and Virtual Environments*, 4(1):24–49, 1995.
21. V. A. Summers, K. S. Booth, T. Calvert, E. Graham, and C. L. MacKenzie. Calibration for Augmented Reality Experimental Testbeds. In *Proceedings ACM Symposium on Interactive 3D Graphics*, pages 155–162, Atlanta, Georgia, Apr. 1999.
22. M. Tuceryan, D. S. Greer, R. T. Whitaker, D. E. Breen, E. Rose, K. H. Ahlers, and C. Crampton. Calibration Requirements and Procedures for a Monitor-Based Augmented Reality System. *IEEE Transactions on Visualization and Computer Graphics*, 1(3):255–273, 1995.
23. L. Vaissie, J. P. Rolland, and G. M. Bochenek. Analysis of Eyepoint Locations and Accuracy of Rendered Depth in Binocular Head-Mounted Displays. In *Proceedings SPIE Stereoscopic Displays and Virtual Reality Systems*, pages 57–64, San Jose, California, Jan. 1999.
24. T. E. von Wiegand, D. W. Schloerb, and W. L. Sachtler. Virtual Workbench: Near-Field Virtual Environment System with Applications. *Presence: Teleoperators and Virtual Environments*, 8(5):492–519, 1999.
25. Z. Wartell, L. F. Hodges, and W. Ribarsky. The Analytic Distortion Induced by False-Eye Separation in Head-Tracked Stereoscopic Displays. Technical Report GIT-GVU-99-01, GVU Center, Georgia Institute of Technology, Jan. 1999.
26. Z. Wartell, L. F. Hodges, and W. Ribarsky. A Geometric Comparison of Algorithms for Fusion Control in Stereoscopic HTDs. *IEEE Transactions on Visualization and Computer Graphics*, 8(2):129–143, 2002.